Geophysical Journal International

Geophys. J. Int. (2015) **202,** 94–101 doi: 10.1093/gji/ggv128

GJI Mineral physics, rheology, heat flow and volcanology

The elastic properties and stability of fcc-Fe and fcc-FeNi alloys at inner-core conditions

Benjamí Martorell,* John Brodholt, Ian G. Wood and Lidunka Vočadlo

Department of Earth Sciences, University College London, Gower Street, London, WC1E 6BT, United Kingdom. E-mail: b.massip@ucl.ac.uk

Accepted 2015 March 12. Received 2015 March 11; in original form 2014 October 20

SUMMARY

The agreement between shear wave velocities for the Earth's inner core observed from seismology with those derived from mineral physics is considerably worse than for any other region of the Earth. Furthermore, there is still debate as to the phase of iron present in the inner core, particularly when alloying with nickel and light elements is taken into account. To investigate the extent to which the mismatch between seismology and mineral physics is a function of either crystal structure and/or the amount of nickel present, we have used *ab initio* molecular dynamics simulations to calculate the elastic constants and seismic velocities (V_p and V_s) of face centred cubic (fcc) iron at Earth's inner core pressures (360 GPa) and at temperatures up to ∼7000 K. We find that V_p for fcc iron (fcc-Fe) is very similar to that for hexagonal close packed (hcp) iron at all temperatures. In contrast, V_s for fcc-Fe is significantly higher than in hcp-Fe, with the difference increasing with increasing temperature; the difference between V_s for the core (from seismology) and V_s for fcc-Fe exceeds 40 per cent. These results are consistent with previous work at lower temperatures. We have also investigated the effect of 6.5 and 13 atm% Ni in fcc-Fe. We find that Ni only slightly reduces V_p and V_s (e.g. by 2 per cent in V_s for 13 atm% Ni at 5500 K), and cannot account for the difference between the velocities observed in the core and those of pure fcc-Fe. We also tried to examine pre-melting behaviour in fcc-Fe, as reported in hcp-Fe by extending the study to very high temperatures (at which superheating may occur). However, we find that fcc-Fe spontaneously transforms to other hcp-like structures before melting; two hcp-like structures were found, both of hexagonal symmetry, which may most easily be regarded as being derived from an hcp crystal with stacking faults. That the structure did not transform to a true hcp phase is likely as a consequence of the limited size of the simulation box (108 atoms). At 360 GPa, in pure fcc-Fe, we find that the transition from fcc to the hcp-like structure occurs at 7000 K, whereas in the Ni bearing system, the transition occurs at higher temperature (7250 K). This reinforces previous work showing that fcc-Fe might transform to hcp-Fe just before melting, and that Ni tends to stabilize the fcc structure with respect to hcp.

Key words: Core, outer core and inner core; Elasticity and anelasticity; High-pressure behaviour; Phase transitions; Wave propagation; Mechanics, theory, and modelling.

1 INTRODUCTION

In the Earth's mantle and outer core, the observed seismological wave velocities can be understood in terms of mineralogical and compositional models, with such models matching the observed velocities to around a percent or so (e.g. Stixrude & Lithgow-Bertelloni 2012; Zhang *et al.* 2013). An exception to this is the *S*-wave velocity of the inner core. Seismology provides values of V_s of between 3.5 and 3.7 km s^{-1} depending on the depth in the inner core, while mineral physics estimates are almost always substantially higher, at around 4.2 to 4.5 km s^{-1} (e.g. Vočadlo *et al.* 2003; Vočadlo 2007; Vočadlo *et al.* 2009; Antonangeli *et al.* 2010; Martorell *et al.* 2013a). This is problematic since studies show that the effect of alloying iron with both Ni (Martorell *et al.* 2013a) and light-elements (Antonangeli *et al.* 2010) is only small, and

* Now at: Deparment of Materials Science, Deregallera Ltd., Unit 2, De Clare Court, Pontywindy Industrial State, Caerphilly, Wales, CF83 3HU, United Kingdom.

cannot account for the 20 to 30 per cent difference in V_s. A number of suggestions for how this remarkably large discrepancy might be reconciled have been proposed—for example partial melting, anelasticity, defects, different mineral phases, and, most recently, a strong pre-melting effect on the shear modulus of iron (Martorell *et al.* 2013b).

Experiments on pure iron at very high pressure (Tateno *et al.* 2010) have indicated that it should adopt the hexagonal close packed (hcp) structure in the inner core. However, while a number of computational studies have also found the hcp structure to be the most stable phase at inner-core conditions (e.g. Vočadlo *et al.* 2003) the differences in energies between hcp and other postulated structures [e.g. face centred cubic (fcc), body centered cubic (bcc), etc.] are extremely small. For example, recent calculations using the quasi-harmonic approximation show that the fcc phase of pure iron may be more stable than the hcp phase beyond 6000 K (Côté *et al.* 2012) at inner-core pressure, in agreement with results from classical molecular dynamics simulations at 6600 K (Ekholm *et al.* 2011). The fcc structure cannot, therefore, yet be fully ruled out as a core-forming phase and so in this paper we address an important missing aspect of the story by calculating the high-temperature elasticity of fcc-Fe and the fcc-FeNi system.

Addition of impurities to Fe can modify both the phase stability and the elastic properties. Although light elements may also be important, the major alloying element in the Earth's inner core is nickel, of which 5–15 wt% is expected to be present. Unfortunately, studies on Fe–Ni alloys have given conflicting results. Static Diamond Anvil Cell (DAC) experiments with 10 wt% Ni in Fe have shown only the hcp structure up to 340 GPa and 4700 K (Tateno *et al.* 2012; Sakai *et al.* 2013), but other studies with different concentrations of Ni (15, 25 and 32 wt%) suggest that Ni favours the fcc structure, although milder conditions (25 GPa, room temperature) were used in these experiments (Shabashov *et al.* 2009). A trend towards increasing fcc stability is also observed in quasi-harmonic calculations on Fe–Ni alloys (Côté *et al.* 2012), but classical molecular dynamics simulations at 6600 K (Ekholm *et al.* 2011) suggest that Ni will destabilize the fcc structure with respect to hcp at 360 GPa.

Although the elasticity of fcc-Fe at high temperature and pressure has been calculated previously using the methods employed here (Vočadlo *et al.* 2008), those calculations were made at core-densities, not at core pressures. This is an important point because the pressure of the simulations was only ∼316 GPa, and so they do not, therefore, necessarily give the properties of Fe under inner-core pressures. Moreover, the simulations only reached 5500 K and it is now considered distinctly possible that the inner core is hotter than was thought in 2008 (Anzellini *et al.* 2013). Higher temperature simulations are needed to determine whether the pre-melting weakening of the elastic constants observed in hcp-Fe (Martorell *et al.* 2013b) also occurs in fcc-Fe.

We have, therefore, performed *ab initio* molecular dynamics (AIMD) simulations of fcc-Fe and fcc-FeNi solid solutions up to their melting temperatures. In summary, we find that V_s is even greater than in hcp-Fe, making the discrepancy with the values for the core from seismology even worse. For pure fcc-Fe, the strong pre-melting weakening seen in hcp-Fe was not observed, but instead the fcc-structure spontaneously transformed to an hcp-type structure before melting. The systems containing Ni showed similar behaviour, also transforming to an hcp-like structure; however, this transformation occurred at a higher temperature, suggesting that Ni stabilizes the fcc structure relative to hcp.

2 METHODS

2.1 Electronic structure calculations

The calculations performed in this work are based on density functional theory (DFT) using the Vienna *ab initio* simulation package (VASP; Kresse & Hafner 1993a,b; Kresse & Hafner 1994). The effect of the core electrons on the valence electrons is described by the projector augmented wave method (PAW; Blöchl 1994; Kresse & Joubert 1999). The generalized gradient approximation was used with the functional of Perdew & Wang (1992). A convergence of the plane-wave expansion was obtained with a cut-off of 400 eV.

We ran finite temperature AIMD. The VASP code uses the Verlet algorithm to integrate the classical Newton's equations of motion. A time step of 1.5 fs was used for the integration. Simulations were performed at constant temperature using an Andersen thermostat, with a restarting value of 150 cycles.

The simulation box for fcc-Fe consisted of a cubic 3 × 3 × 3 supercell of the 4-atom face-centred cubic cell of the fcc structure (108 atoms in total). A k-point grid of two irreducible *k*-points was used. For fcc-$Fe_{0.935}Ni_{0.065}$ and fcc-$Fe_{0.87}Ni_{0.13}$, 7 and 17 Fe atoms in the fcc-Fe structure were, respectively, systematically substituted by Ni atoms in the most dispersed way possible.

Simulations were performed at nominal temperatures of: 0, 2000, 5500, 6000, 6500, 6750, 7000 and 7500 K for fcc-Fe; 0 and 5500 K for fcc-$Fe_{0.935}Ni_{0.065}$; 0, 5500, 7000 and 7500 K for fcc-$Fe_{0.87}Ni_{0.13}$. Simulations were run for between 10 and 15 ps. The actual temperature of the simulation was determined from an average excluding the first 2 ps of the simulation. Stresses were determined as outlined below. To ensure that we were computing the stresses of solid phases, we retrieved the mean-square displacements (MSD) for the last 5 ps of each simulation.

2.2 Elastic properties

In order to obtain the elastic properties of the fcc structures we used the same procedure as for hcp-Fe (Martorell *et al.* 2013a,b). In summary, we first optimized the unit-cell parameters and densities using VASP simulations in the isothermal-isobaric ensemble (NPT ensemble) using the barostat implemented in VASP by Hernández (Souza & Martins 1997; Hernández 2001); we ran this simulation for up to 5 ps. The average lattice parameters from these NPT simulations were then used to create a unit cell to which distortions were applied (see below); the stresses on the simulation box were then obtained from VASP simulations in the canonical ensemble (NVT ensemble) run over ∼10–15 ps.

Once the equilibrium structure of each system was obtained, the elastic constants, c_{ij}, were evaluated by distorting the unit cells according to the distortion matrix shown below:

$$\begin{pmatrix} 1+\delta & \delta/2 & 0 \\ \delta/2 & 1 & 0 \\ 0 & 0 & 1 \end{pmatrix}.$$

Using the time-averaged stresses from the calculations, the elastic constants were obtained by the standard relation $\sigma_{ij} = c_{ijkl}\epsilon_{kl}$. The calculated stresses on the simulation box for four different strains (±0.01 and ±0.02) were fitted to second-order polynomials, and their slopes evaluated at zero strain, thereby determining the stress–strain relationship in the limit of unchanged (i.e. constant) volume (Karki *et al.* 2001); this method has been widely used previously for determining elastic constants of many geophysical systems such as $MgSiO_3$ perovskite (Oganov *et al.* 2001).

As discussed in Vočadlo (2007), we use the Voigt average (Simmons & Wang 1971) to calculate the elastic properties of the polycrystalline aggregate (incompressibility: K; shear modulus: G) which are given by:

$$K_{\mathrm{T}} = \frac{c_{11} + 2c_{12}}{3};\ G = \frac{3c_{44} + c_{11} - c_{12}}{5}. \quad (1)$$

Finally, we obtained the adiabatic incompressibility, K_{S}, from the relation

$$K_{\mathrm{s}} = K_T(1 + \alpha\gamma T) \quad (2)$$

using values of the volumetric thermal expansion coefficient, $\alpha = 10^{-5}\ \mathrm{K}^{-1}$ and the Grüneisen parameter, $\gamma = 1.5$ (Vočadlo *et al.* 2003; Vočadlo 2007). The isotropic wave propagation velocities in the material can then be evaluated from the bulk and shear moduli, and the density, ρ, as follows:

$$V_{\mathrm{p}} = \sqrt{\frac{K + \frac{4}{3}G}{\rho}};\ V_{\mathrm{s}} = \sqrt{\frac{G}{\rho}}. \quad (3)$$

2.3 Temperature dependence of the shear modulus and estimate of melting temperature

We used the Nadal-Le Poac (NP) shear modulus model, based on Lindemann melting theory, to describe the temperature dependence of G at a fixed pressure (Nadal & Le Poac 2003). This takes the form:

$$G(P,T) = \frac{1}{J(T)}\left[\left(G_0 + \frac{\partial G}{\partial P}\frac{P}{\sqrt[3]{\eta}}\right)\left(1 - \frac{T}{T_{\mathrm{m}}}\right) + \frac{\rho}{C\mathrm{m}}k_{\mathrm{b}}T\right], \quad (4)$$

where

$$C = \frac{(6\pi)^{2/3}}{3}f^2, \quad (5)$$

$$J(T) = 1 + \exp\left[-\frac{1 + 1/\zeta}{1 + \zeta/\left(1 - \frac{T}{T_{\mathrm{m}}}\right)}\right] \quad (6)$$

and

$$G_{\mathrm{p}} = G_0 + \frac{\partial G}{\partial P}\frac{P}{\sqrt[3]{\eta}}. \quad (7)$$

In eqs 4–7, G is the shear modulus, P is the pressure, T is the temperature, G_0 is the shear modulus at 0 K and 0 GPa, η is the compression (the ratio of the density under pressure to that at ambient pressure), T_{m} is the melting temperature, ρ is the density, m is the atomic mass, k_{b} is the Boltzmann constant, f is the Lindemann constant for the material and ζ is a material parameter. We have fitted our results to this model with four adjustable parameters, that is, C, ζ, T_{m} and G_{P} (within the model, $\partial G/\partial P$ and η are assumed to be temperature independent and, since our calculations are at constant P, G_{P} may be taken as a constant). With this model we can estimate the mechanical melting temperature of the material and its Lindemann constant. This latter value is in the range of 0.1–0.3 for most materials. When applying the NP model to velocities (substituting G with V), we refer to it in the text as an 'NP-like' model.

3 RESULTS AND DISCUSSIONS

In the first part of this section we present the results for pure fcc-Fe at 360 GPa as a function of temperature up to 7500 K. We describe the structures, densities and elastic properties and the fit to the NP model (Nadal & Le Poac 2003) for the shear modulus (G) as a function of temperature. In the second part we present the effect of Ni on the elastic properties of fcc-Fe and discuss how Ni can affect the stability field of fcc-Fe at 360 GPa and at temperatures up to 7500 K.

3.1 AIMD simulations of fcc-Fe at 360 GPa up to 7500 K

As described in Section 1.2, we first performed NPT simulations at 5500, 6500, 7000 and 7500 K to obtain the density. For simulations at 5500 and 6500 K, we obtained the optimized lattice parameter as expected; however, for simulations at 7000 and 7500 K, an unexpected result was obtained—the cubic lattice was lost and a new dimensionally orthorhombic lattice and unit cell (later found to be a C-centred cell of a structure with hexagonal symmetry) was obtained. This implies that the fcc-Fe structure is dynamically unstable at 7000 K and above. To confirm this result, we performed a constant-volume calculation for fcc-Fe at 7000 K with the unit cell constrained to be cubic; in this case fcc-Fe melted. This is a clear indication that, for simulations at 360 GPa, fcc-Fe is thermodynamically less stable than hcp-Fe, which remains solid at this temperature (Martorell *et al.* 2013b).

3.1.1 Structural transitions

Analysis of the new structure formed at 7000 K revealed that the simulated, $a = 9.048$ Å, cubic supercell (formed from $3 \times 3 \times 3$ 4-atom fcc unit cells, with $a = 3.016$ Å when cubic symmetry is enforced) had turned into a dimensionally orthorhombic supercell with $a = 6.348$ Å, $b = 11.151$ Å and $c = 10.455$ Å (Fig. 1). These unit-cell vectors imply that the dimensions of the cells from which the supercell was constructed have become $a = 2.116$, $b = 3.717$ and $c = 3.485$ Å. Inspection of these values showed that they were very similar to those in our previous calculations of hcp-Fe; there we used a simulation box based on $4 \times 2 \times 2$ C-centred, 4-atom, dimensionally orthorhombic hcp unit cells with $a = 2.133$ Å, $b = 3.711$ Å and $c = 3.466$ Å at 7000 K (Martorell *et al.* 2013b). The similarity in cell parameters (small differences are expected from the

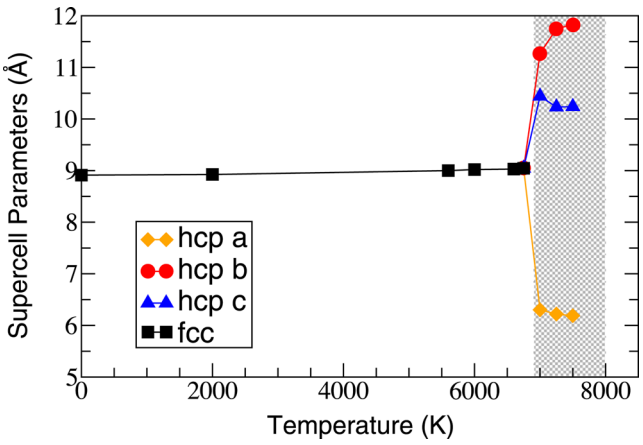

Figure 1. Calculated supercell parameters fcc-Fe (black squares) as a function of temperature at 360 GPa. Beyond 6750 K, the three parameters diverge to a dimensionally orthorhombic structure with different vectors a (yellow diamonds), b (red circles) and c (blue triangles). The grey band represents the minimum and maximum melting temperatures presented in the paper of Morard *et al.* (2011, and references therein) for hcp-Fe at 360 GPa.

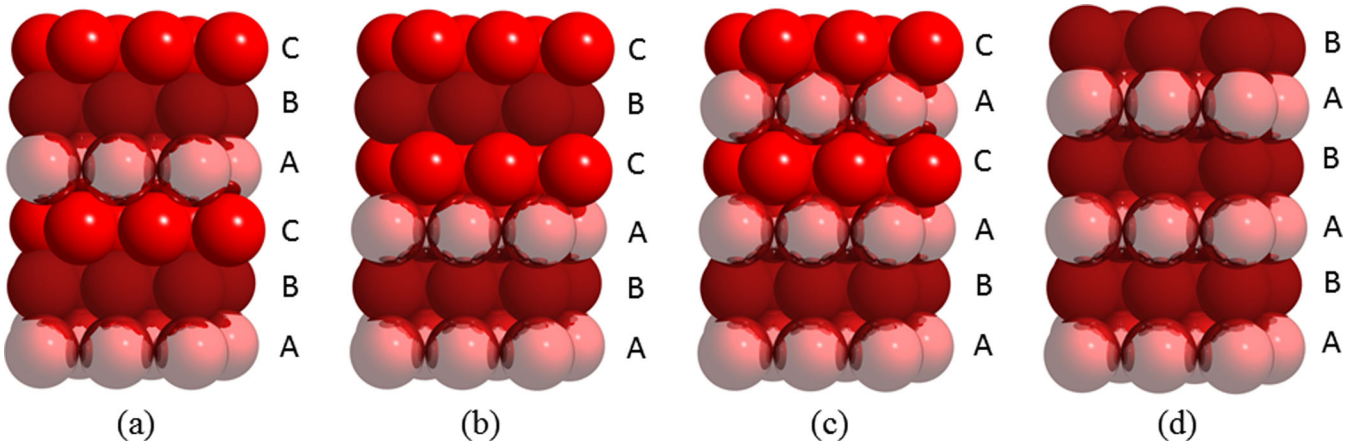

Figure 2. Stacking sequence of close-packed planes for (a) fcc and (d) hcp structures, together with the new structures found in this work at 7000 K (b) and at 7250 K and 7500 K (c). These are the only physically distinct structures that can be formed by stacking close-packed layers, such that the number of layers in the periodically repeating unit is two, three or six.

different k-points grid used) indicated that the new structure was clearly related to an hcp-like stacking. A more detailed analysis of the 7000 K simulation revealed a stacking sequence of 6 close-packed planes in the periodically repeating unit in the order ABACBC; at higher temperatures (7250 K and 7500 K) the order was ABACAC (Fig. 2). The ideal symmetry of these two new structures was determined using the program Endeavour (Putz *et al.* 1999) from atomic coordinates corresponding to the stacking of perfect close-packed planes of spheres. This revealed that the ABACBC sequence has space group $P6_3/mmc$ with $c \sim 3\sqrt{(8/3)}a$, $Z = 6$, and atoms in the $2b$ (0, 0, $\frac{3}{4}$) and $4f$ (1/3, 2/3, 7/12) sites. The symmetry is thus unchanged from that of simple hexagonal close packing, although the unit cell volume is, of course, three times larger. The ABACAC sequence has space group $P\bar{6}m2$ ($c \sim 3\sqrt{(8/3)}a, Z = 6$) and atoms in the $1b$ (0, 0, $\frac{1}{2}$), $1e$ (2/3, 1/3, 0), $2g$ (0, 0, 5/6) and $2h$ (1/3, 2/3, 1/3) sites. These new structures are similar to the hcp (AB) or d-hcp structures (ABAC), and we therefore refer to them from here onwards as 'hcp-like' structures. The fact that we did not obtain the ideal hcp structure in our simulations is probably a consequence of the multiple degrees of freedom in the phase transition, the high mobility of the atoms in the phase transition, which occurs close to the melting point of hcp-Fe, and the finite size of the simulation box, which limits the maximum number of close-packed planes in the stacking sequence to six. Further consideration of all possible stacking sequences of close-packed layers, commensurate with a maximum repeating unit of six layers, revealed that the four structures shown in Fig. 2 are, in fact, the only such structures that can be formed, as all other possible arrangements (e.g. ABABAC, etc.) are equivalent to either ABACBC or ABACAC.

The transitions from the fcc to the hcp-like structures in these simulations can be explained and summarized in three steps (Fig. 3) that occur simultaneously: (1) the unit-cell vectors of the simulation box contract (a) and expand (b and c) to the values previously discussed (see Fig. 1), such that $b \sim \sqrt{3}a$; (2) due to the change in a and b, the non-close-packed (001) planes of the fcc structure undergo a transformation into the close packed (0001) planes of the hcp-like structures, as was found by Li *et al.* (2010) for Al crystals. Within a single non-close-packed (001) plane of the fcc structure, no change in fractional coordinates is required because the change in the unit cell vectors inevitably results in the plane becoming close packed (see Fig. 3); thus, for example atoms in the plane at $z = 0$ have the same fractional coordinates (0, 0, 0 and $\frac{1}{2}$, $\frac{1}{2}$, 0 for an fcc sub-cell) in both the fcc and hcp-like structures; (3) the new close-packed planes are then displaced within (0001) so as to stack in the ABACBC or ABACAC sequences (see Fig. 2). Given the nature of the transition mechanism, the fact that the simulations at 7000 K and at 7250 and 7500 K produced different structures is probably not significant, although it is interesting to note that the simulations below 7000 K have all layers of atoms in a cubic close packed (ccp) environment, that at 7000 K has four of the six layers in a ccp environment and two in an hcp environment, whereas those at 7250 and 7500 K have four of the six layers in an hcp environment and two in a ccp environment.

Although our results suggest that fcc-Fe will transform to the hcp structure at around 7000 K, this is probably above the thermodynamic melting temperature of both phases. The range of likely melting temperatures from computer simulations for hcp-Fe at 360 GPa, using the coexistence method, is ~6600–7300 K (Alfè 2009; Sola & Alfè 2009); as far as we are aware, no similar calculations have been performed for fcc-Fe. In the present case, our simulations involve periodic boundary conditions and a relatively small numbers of atoms which can lead to an overestimate of the melting temperature (e.g. Bouchet *et al.* 2009); this is probably because there are no free surfaces or impurities in the structure on which to initiate defects which can then propagate into the solid. In our simulations we can introduce defects into the bulk solid only by thermal activation which leads to overheating. However, if it is the homologous temperature which is important, rather than the absolute temperature, our results may still represent the true behaviour of the material very close to T_m. This issue, however, requires further investigation. A larger supercell may allow both melting and the transition between fcc and hcp-like structures to occur at lower temperatures, perhaps because of a better description of the anharmonic properties.

The possibility that the Earth's inner core consists of a defective hexagonal close-packed structure with planar stacking faults, similar to those found in the present work, has been discussed previously by Ishikawa *et al.* (2011). They examined all possible structures formed by stacking of close-packed planes commensurate with a supercell containing 12 close-packed layers (including those described here). They proposed that the production of defective structures by thermally activated lateral sliding of the close-packed layers could contribute to both seismic anisotropy and seismic attenuation. The fact that these stacking faults occur so readily

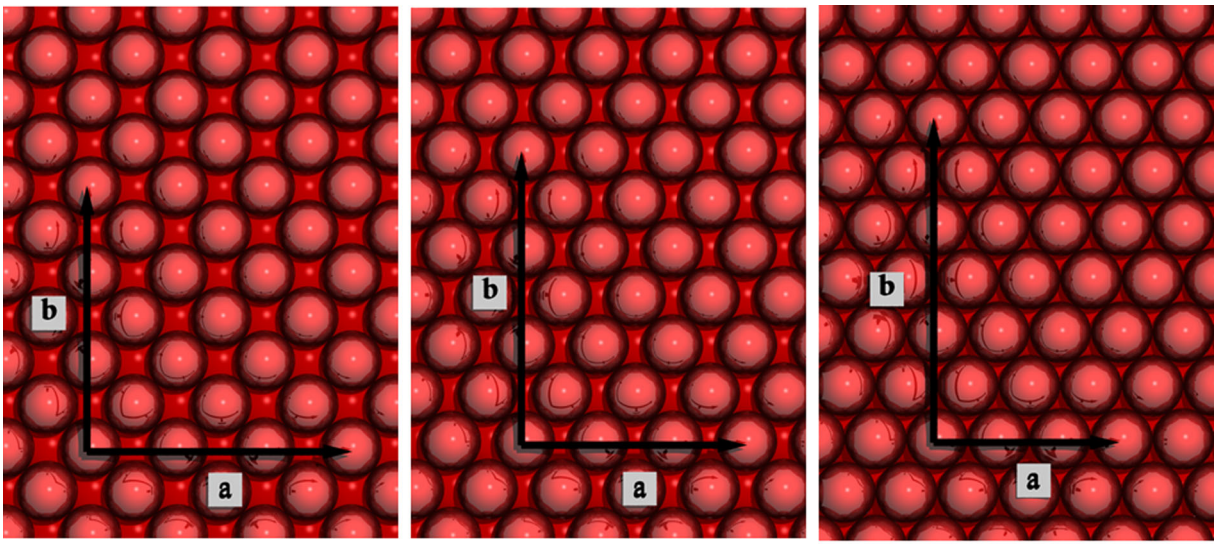

Figure 3. Evolution of the supercell parameters and atomic positions during the transition from the fcc structure to an hcp-like structure of Fe at 360 GPa. (a) The non-close-packed (001) plane of the fcc structure. (b) Hypothetical intermediate structure of this plane in the fcc-hcp transition. (c) The close-packed (0001) plane in the hcp structure.

in our simulations reinforces the suggestion of Ishikawa *et al.* (2011) that stacking faults could occur in large concentrations in the core. The importance of defects for inner-core properties has also been discussed by Belonoshko *et al.* (2007) on the basis of classical computer simulations of body-centred-cubic iron. It was found that the shear modulus and shear wave velocity were dramatically lower than those of the defect-free solid and that atomic diffusion was greatly increased (Belonoshko *et al.* 2010). Whether such effects occur in hcp-Fe at inner-core conditions, however, is yet to be established.

3.1.2 Elastic constants

We performed the elastic constant calculations at 0, 2000, 5500 6000, 6500 and 6750 K at the optimized lattice parameters for each temperature. At 6750 K, three of the strained points ($\varepsilon = \pm 2$ per cent and -1 per cent) melted during the NVT simulation and so we analysed the strain–stress (σ–ε) curve with only two points ($\varepsilon =$ 0 per cent, 1 per cent). The results at 6750 K, however, seem to follow the same trend as our calculations at lower temperatures (see Fig. 4). In particular there is no indication of a strong pre-melting weakening as seen in our earlier calculations on hcp-Fe (Martorell *et al.* 2013b). It is possible that this is because the unstrained fcc structures preferred to transform to the hcp-like structure before melting. As mentioned earlier, simulations at 7000 K with the structure fixed in the cubic setting melted, which we interpret as indicating instability with respect to the hcp-like structure.

In Table 1 we present the elastic constants for fcc-Fe, together with the values for hcp-Fe from previous work (Martorell *et al.* 2013b). As expected, the elastic constants for fcc-Fe decrease with temperature to 6750 K, with c_{11} and c_{44} being the most affected. When comparing the values for fcc-Fe with those for hcp-Fe, we observe that, at equivalent temperatures, c_{11} is always smaller for fcc than for hcp (in this case c_{11} for fcc must be compared with c_{11} and c_{33} for hcp), whereas c_{12} and c_{44} are slightly larger and much larger, respectively (again, c_{12} for fcc must be compared with c_{12} and c_{13} for hcp). This behaviour is in agreement with the results from calculations performed previously for fcc and hcp-Fe

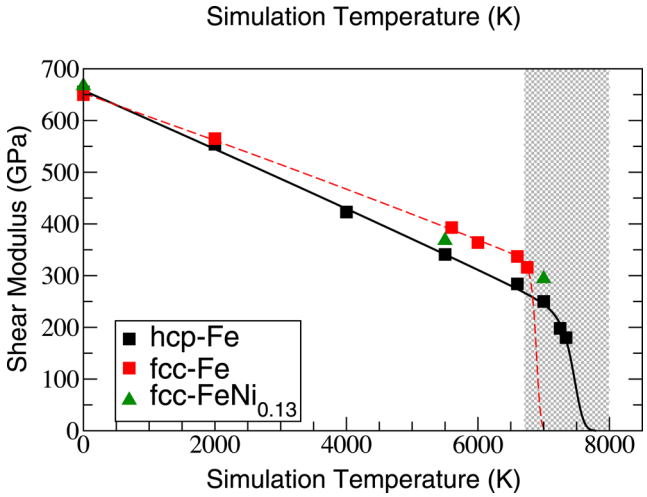

Figure 4. Calculated shear modulus for fcc-Fe (red squares) as a function of temperature at 360 GPa. The red dashed line is the NP model fitted to the calculated shear modulus. The black line is the NP model for hcp-Fe for comparison. The green triangles indicate the shear modulus of fcc-$Fe_{0.87}Ni_{0.13}$. The grey band represents the minimum and maximum melting temperatures presented in the paper of Morard *et al.* (2011 and references therein) for hcp-Fe at 360 GPa.

at 5500 K and 13 155 kg m^{-3} (∼316 GPa for pure iron; Vočadlo *et al.* 2008).

We have applied the NP model to the shear moduli obtained from our calculations for fcc-Fe. The fit is shown in Fig. 4, together with results for hcp-Fe for comparison (Martorell *et al.* 2013b). We obtained a melting temperature (T_m) and a Lindemann parameter (f) for fcc-Fe of 6885 K and 0.092, respectively. The values for hcp-Fe are larger, 7475 K and 0.115. Although this is a simplistic model for obtaining melting temperatures, it supports the suggestion that fcc-Fe melts at a lower temperature than hcp-Fe at 360 GPa, indicating that fcc-Fe is a thermodynamically less stable phase than hcp-Fe. A consequence of the methodology is, however, that these melting temperatures will be overestimated since there is no surface at which

Table 1. Elastic properties and densities for fcc-Fe and fcc-FeNi alloys at 360 GPa. Re-evaluated elastic properties of hcp-Fe and PREM at 360 GPa are given for comparison.

	T_{final} (K)	ρ (kg m^{-3})	c_{11} (GPa)	c_{12}	c_{33}	c_{13}	c_{44}	K_s (GPa)	G	V_p (km s^{-1})	V_s
hcp-Fe[a]	0	14185	2493	1151	2689	1085	577	1590	655	13.18	6.80
	2000	14138	2356	1282	2571	1083	476	1622	554	12.92	6.26
	4000	13880	2092	1292	2275	1063	351	1566	423	12.39	5.52
	5500	13739	1942	1303	2097	1077	276	1546	341	12.07	4.98
	6600	13628	1803	1297	2067	1132	232	1560	284	11.93	4.57
	7000	13529	1708	1289	1890	1060	202	1489	250	11.60	4.29
	7250	13495	1653	1384	1824	1046	151	1488	198	11.39	3.82
	7340	13482	1579	1399	1786	1013	153	1454	180	11.21	3.65
fcc-Fe	0	14156	2037	1377			863	1598	650	13.19	6.77
	2000	14094	1949	1375			750	1610	565	12.96	6.33
	5600	13743	1641	1298			541	1529	393	12.22	5.35
	6000	13652	1555	1288			517	1501	364	12.06	5.16
	6600	13611	1557	1349			492	1556	337	12.13	4.97
	6750	13540	1465	1320			479	1507	316	11.94	4.83
fcc-$FeNi_{0.065}$	0	14214	2062	1364			858	1597	654	13.18	6.79
	5500	13781	1646	1341			524	1562	375	12.21	5.22
fcc-$FeNi_{0.13}$	0	14278	2083	1365			872	1604	667	13.21	6.83
	5500	13830	1593	1330			526	1535	368	12.10	5.16
	7000	13515	1436	1302			445	1488	294	11.79	4.66
PREM[b]		13090						1425	176	11.26	3.67

[a]The values given here for hcp-Fe are slightly different from those reported in our previous work (Martorell *et al.* 2013b) in that: (i) we now have values at 4000 K, (ii) we re-ran the 5500 K simulation point, (iii) we continued the simulations at 6600 K and 7000 K for longer and (iv) we discarded some strained simulations at 7250 K and 7340 K which we later found had melted; the overall results and conclusions, however, are in full agreement with Martorell *et al.* (2013b).
[b]Dziewonski & Anderson (1981). Errors in c_{ij} and velocities are below 2 per cent.

to nucleate melting. Our AIMD results, therefore, do not support the quasi-harmonic lattice dynamics calculations on Fe and Fe–Ni alloys, where it was suggested that fcc structure could be more stable than hcp beyond 6000 K (Côté *et al.* 2012), or the classical molecular dynamics simulations which showed that the fcc structure was more stable than hcp at 360 GPa and 6600 K (Ekholm *et al.* 2011).

One possibility for why our results predict hcp to be stable up to T_m, while those of Côté *et al.* (2012) predict fcc to become stable before melting, could be anharmonicity. Our AIMD simulations directly include anharmonicity whereas the lattice dynamics of Côté *et al.* (2012) are only at the quasi-harmonic level. Since anharmonicity becomes increasingly important at high temperatures—especially so near the T_m—the difference can be explained by subtle differences in the anharmonic contributions to fcc and hcp phases, not included in the work of Côté *et al.* (2012). The difference between our results and those of Ekholm *et al.* (2011) may be explained by the fact that they use classical potential models whereas we use DFT. Given that we expect DFT to be more exact than classical potentials (even when those potentials are obtained from fits to DFT results) we suggest that our results are more likely to be correct.

In Fig. 5 we plot *P*- and *S*-wave velocities for fcc-Fe and hcp-Fe at 360 GPa as a function of temperature, fitted to 'NP-like' models as before. We observe that the compressional velocities (V_p) for the fcc and hcp structures are very similar, with V_p decreasing from 13.19 to 11.94 km s^{-1} between 0 K and 6750 K. On the other hand, the temperature dependence of V_s for fcc is somewhat less than that for hcp. At 0 K, V_s is very similar for fcc and hcp structures (6.77 and 6.80 km s^{-1}, respectively), but at 6600 K V_s for fcc-Fe is about 9 per cent larger than for hcp. This exacerbates the difference between the shear-velocity values for the inner core from seismology and those of Fe under similar conditions, with V_s for fcc-Fe exceeding that obtained from seismology by about 40 per cent.

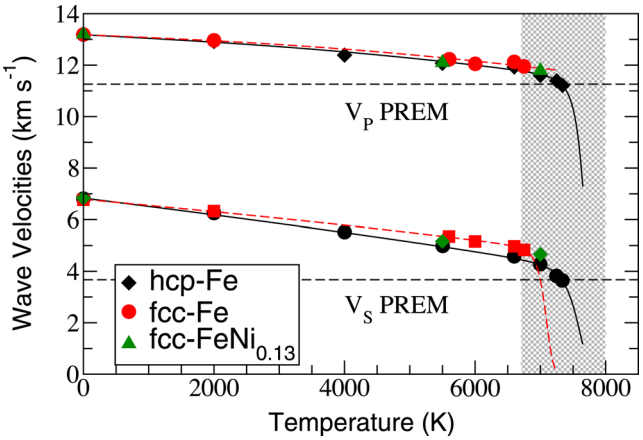

Figure 5. Calculated compressional (red circles) and shear wave (red squares) velocities for fcc-Fe as a function of temperature at 360 GPa. The red dashed lines are the NP-like models fitted to the velocities. The black symbols and lines are the results for hcp-Fe for comparison. The green triangles and green diamonds indicate V_p and V_s for $Fe_{0.87}Ni_{0.13}$. The grey band represents the minimum and maximum melting temperatures presented in the paper of Morard *et al.* (2011 and references therein) for hcp-Fe at 360 GPa.

3.2 AIMD simulations of fcc-FeNi at 360 GPa

In a recent work we have shown that Ni has a very small effect on the wave propagation velocities in hcp-Fe at 360 GPa, especially at high temperature (1 per cent reduction in V_s at 5500 K; Martorell *et al.* 2013a). Although there is no strong reason to suspect that the effect of Ni will be different for fcc-Fe, this has yet to be demonstrated. Here, we show in Table 1 the elastic properties of fcc-FeNi alloys, with 6.5 per cent and 13 per cent molar fraction of Ni, at 0 and

5500 K; for the 13 per cent composition we have also calculated the elastic properties at 7000 K.

At 0 K our results agree well with those published by Asker *et al.* (2009), using calculations based on muffin-tin orbital methods, who obtained a value for G for pure fcc-Fe at 360 GPa of 670 GPa (650 GPa in our case). On addition of nickel, they observe a slight decrease in G to 650 GPa for a fcc 20 per cent Ni alloy while our G is slightly increased to 667 GPa, probably due to the different method used in the electronic structure calculations.

At 5500 K and 360 GPa, the addition of Ni only slightly reduces V_p and V_s from the values for pure fcc-Fe; for example, 13 atm% Ni reduces V_p and V_s by 1 and 3 per cent, respectively. These small reductions cannot account for the large discrepancy between seismological observations and the values for pure fcc-Fe. Our velocity reductions are of the same order of magnitude as those found in sound velocity measurements performed at lower pressures and temperatures by Lin *et al.* (2003) in hcp-$Fe_{0.92}Ni_{0.08}$ at 106 GPa and room temperature, and by Kantor *et al.* (2007) in fcc-$Fe_{0.78}Ni_{0.22}$ at 72 GPa and 715 K; in both cases no significant deviations in V_p and V_s were observed on addition of Ni.

We also explored the behaviour of Fe–Ni alloys at higher T in the region of the transitions from fcc to hcp-like phases discussed in Section 2.1 by performing simulations at 7000 and 7500 K for 13 atm% Ni. The NPT calculation at 7500 K resulted in the same behaviour as for pure fcc-Fe, that is the fcc-FeNi alloy transformed to an hcp-like structure. However, at 7000 K this transformation did not occur. This suggests that Ni not only thermodynamically stabilizes fcc-Fe, but also stabilizes it dynamically. We were able, therefore, to obtain the elastic properties of the fcc-FeNi alloy at 7000 K (Table 1), which had not been possible in the case of pure fcc-Fe. These results are plotted, together with the values for hcp- and fcc-Fe in Figs 4 and 5. Because the effect of Ni on the elastic properties of fcc-Fe is small, we observe that G (Fig. 4), V_p and V_s (Fig. 5) for fcc-$Fe_{0.87}Ni_{0.13}$ at 360 GPa and 7000 K are consistent with the linear region of pure fcc-Fe. Even at 7000 K, therefore, the fcc-$Fe_{0.87}Ni_{0.13}$ alloy does not show any pre-melting shear weakening and the shear wave velocity is still significantly faster (∼40 per cent) than that found in the core.

4 CONCLUSIONS

We have computed the elastic properties of pure fcc-Fe at 360 GPa up to 7500 K and studied the effect of the addition of Ni on its structural and elastic properties. Compressional velocities for fcc-Fe are very similar to those of hcp-Fe up to 6750 K, but V_s is slightly larger for fcc-Fe than for hcp-Fe up to 6750 K. Beyond this point, fcc-Fe becomes dynamically unstable and converts to hcp-like structures. Fe in the fcc phase does not, therefore, show the same pre-melting weakening seen in hcp Fe (Martorell *et al.* 2013b). Using the NP shear modulus model we have estimated that the melting temperature of fcc-Fe is significantly lower than that for hcp-Fe. We find that Ni has only a small effect on the elastic properties of fcc-Fe, but does stabilize the fcc structure up to about 7000 K.

ACKNOWLEDGEMENTS

This work was supported by NERC grant NE/H003975/1 awarded to LV. Calculations were performed in the HECTOR supercomputer facility.

REFERENCES

Alfè, D., 2009. Temperature of the inner-core boundary of the Earth: melting of iron at high pressure from first-principles coexistence simulations, *Phys. Rev. B,* **79,** 60 101–60 104.

Antonangeli, D., Siebert, J., Badro, J., Farber, D.L., Fiquet, G., Morard, G. & Ryerson, F.J., 2010. Composition of the Earth's inner core from high-pressure sound velocity measurements in Fe-Ni-Si alloys, *Earth Planet. Sci. Lett.,* **295,** 292–296.

Anzellini, S., Dewaele, A., Mezouar, M., Loubeyre, P. & Morard, G., 2013. Melting of Iron at Earth's Inner Core Boundary Based on Fast X-ray Diffraction, *Science,* **340,** 464–466.

Asker, C., Vitos, L. & Abrikosov, I.A., 2009. Elastic constants and anisotropy in FeNi alloys at high pressures from first-principles calculations, *Phys. Rev. B,* **79,** 21 4112–21 4119.

Belonoshko, A.B., Skorodumova, N.V., Davis, S., Osiptsov, A.N., Rosengren, A. & Johansson, B., 2007. Origin of the low rigidity of the Earth's inner core, *Science,* **316,** 1603–1605.

Belonoshko, A.B., Bryk, T. & Rosengren, A., 2010. Shear relaxation in iron under the conditions of Earth's inner core, *Phys. Rev. B,* **104,** 245703.

Blöchl, P.E., 1994. Projector augmented-wave method, *Phys. Rev. B,* **50,** 17 953–17 979.

Bouchet, J., Bottin, F., Jomard, G. & Zérah, G., 2009. Ab initio melting curve of aluminum, *Phys. Rev. Lett.,* **80,** 94 102–94 112.

Côté, A.S., Vočadlo, L. & Brodholt, J.P., 2012. *Ab initio* simulations of iron-nickel alloy at Earth's core conditions, *Earth planet. Sci. Lett.,* **345–348,** 126–130.

Dziewonski, A.M. & Anderson, D.L., 1981. Preliminary reference Earth model, *Phys. Earth planet. Inter.,* **25,** 297–356.

Ekholm, M., Mikhaylushkin, A.S., Simak, S.I., Johansson, B. & Abrikosov, I.A., 2011. Configurational thermodynamics of Fe-Ni alloys at Earth's core conditions, *Earth planet. Sci. Lett.,* **308,** 90–96.

Hernández, E., 2001. Metric-tensor flexible-cell algorithm for isothermal isobaric molecular dynamics simulations, *J. Chem. Phys.,* **115,** 10 282–10 290.

Ishikawa, T., Tsuchiya, T. & Tsuchiya, J., 2011. Stacking disordered phase of iron in the Earth's inner core from first principles, *Phys. Rev. B,* **83,** 212101.

Kantor, A.P. *et al.*, 2007. Sound wave velocities of fc Fe-Ni alloy at high pressure and temperature by mean of inelastic X-ray scattering, *Phys. Earth planet. Inter.,* **164,** 83–89.

Karki, B.B., Stixrude, L. & Wentzcovitch, R.M., 2001. High-pressure elastic properties of major materials of earth's mantle from first principles, *J. Geophys.,* **39,** 507–534.

Kresse, G. & Hafner, J., 1993a. *Ab initio* molecular dynamics for liquid metals. *Phys. Rev. B,* **47,** 558–561.

Kresse, G. & Hafner, J., 1993b. *Ab initio* molecular dynamics for open-shell transition metals, *Phys. Rev. B,* **48,** 13 115–13 118.

Kresse, G. & Hafner, J., 1994. *Ab initio* molecular-dynamics simulation of the liquid-metal-amorphous-semiconductor transition in germanium, *Phys. Rev. B,* **49,** 14 251–14 269.

Kresse, G. & Joubert, D., 1999. From ultrasoft pseudopotentials to the projector augmented-wave method, *Phys. Rev. B,* **59,** 1758–1775.

Li, L., Shao, J.L., Duan, S.Q. & Liang, J.Q., 2010. Atomistic simulation of the fcc-hcp transition in single-crystal Al under uniaxial loading, *New J. Phys.,* **12,** 033011–13.

Lin, J.-F. *et al.*, 2003. Sound velocities of iron-nickel and iron-silicon alloys at high pressures, *Geophys. Res. Lett.,* **30,** 11–14.

Martorell, B., Brodholt, J., Wood, I.G. & Vočadlo, L., 2013a. The effect of nickel on the properties of iron at the conditions of Earth's inner core: *Ab initio* calculations of seismic wave velocities of Fe-Ni alloys, *Earth planet. Sci. Lett.,* **365,** 143–151.

Martorell, B., Vočadlo, L., Brodholt, J. & Wood, I.G., 2013b. Strong pre-melting effect in the elastic properties of hcp-Fe under inner-core conditions, *Science,* **342,** 466–468.

Morard, G., Bouchet, J., Valencia, D., Mazevet, S. & Guyot, F., 2011. The melting curve of iron at extreme pressures: implications for planetary cores, *High Energ. Den. Phys.,* **7,** 141–144.

Nadal, M.-H. & Le Poac, P., 2003. Continuous model for the shear modulus as a function of pressure and temperature up to the melting point: analysis and ultrasonic validation, *J. Appl. Phys.*, **93,** 2472–2480.

Oganov, A.R., Brodholt, J.P. & Price, G.D., 2001. Ab initio elasticity and thermal equation of state of $MgSiO_3$ perovskite, *Earth planet. Sci. Lett.,* **184,** 555–560.

Perdew, J.P. & Wang, Y., 1992. Accurate and simple analytic representation of the electron-gas correlation energy, *Phys. Rev. B,* **45,** 13 244–13 249.

Putz, H., Schön, J.C. & Jansen, M., 1999. Combined method for *ab initio* structure solution from powder diffraction data, *J. Appl. Crystallogr.,* **32,** 864–870.

Sakai, T., Takahashi, S., Nishitani, N., Mashino, I., Ohtani, E. & Hirao, N., 2013. Equation of state of pure iron and $Fe_{0.9}Ni_{0.1}$ up to 3 Mbar, *Phys. Earth planet. Inter.,* **228,** 114–126.

Shabashov, V.A., Zamatovskii, A.E. & Pilyugin, V.P., 2009. Accomodation stresses and structural-phase transitions in Fe-Ni alloys upon compression in Bridgman Anvils, *Phys. Metal and Metallog+,* **108,** 475–483.

Simmons, G. & Wang, H., 1971. *Single Crystal Elastic Constants and Calculated Aggregate Properties: A Handbook,* MIT Press.

Sola, E. & Alfè, D., 2009. Melting of iron under Earth's core conditions from diffusion Monte Carlo free energy calculations, *Phys. Rev. Lett.,* **103,** 078501.

Souza, I. & Martins, J.L., 1997. Metric tensor as the dynamical variable for variable-cell-shape molecular dynamics, *Phys. Rev. B,* **55,** 8733–8742.

Stixrude, L. & Lithgow-Bertelloni, C., 2012. Geophysics of chemical heterogeneity in the mantle, *Annu. Rev. Earth planet. Sci.,* **40,** 569–595.

Tateno, S., Hirose, K., Ohishi, Y. & Tatsumi, Y., 2010. The structure of iron in Earth's inner core, *Science,* **330,** 359–361.

Tateno, S., Hirose, K., Komabayashi, T., Ozawa, H. & Ohishi, Y., 2012. The structure of Fe-Ni alloy in Earth's inner core, *Geophys. Res. Lett.,* **39,** L12 305–L12 304.

Vočadlo, L., 2007. *Ab initio* calculations of the elasticity of iron alloys at inner core conditions: evidence for a partially molten inner core?, *Earth planet. Sci. Lett.,* **254,** 227–232.

Vočadlo, L., Alfè, D., Gillan, M.J. & Price, G.D., 2003. The properties of iron under core conditions from first principles calculations, *Phys. Earth planet. Inter.,* **140,** 101–125.

Vočadlo, L., Wood, I.G., Alfè, D. & Price, G.D., 2008. *Ab initio* calculations of the free energy and high P-T elasticity of face-centred-cubic iron, *Earth planet. Sci. Lett.,* **268,** 444–449.

Vočadlo, L., Dobson, D. & Wood, I.G., 2009. *Ab initio* calculations of the elasticity of hcp-Fe as a function of temperature at inner-core pressure, *Earth planet. Sci. Lett.,* **288,** 534–538.

Zhang, Z., Stixrude, L. & Brodholt, J., 2013. Elastic properties of $MgSiO_3$-perovskite under lower mantle conditions and the composition of the deep Earth, *Phys. Earth planet. Inter.,* **379,** 1–12.